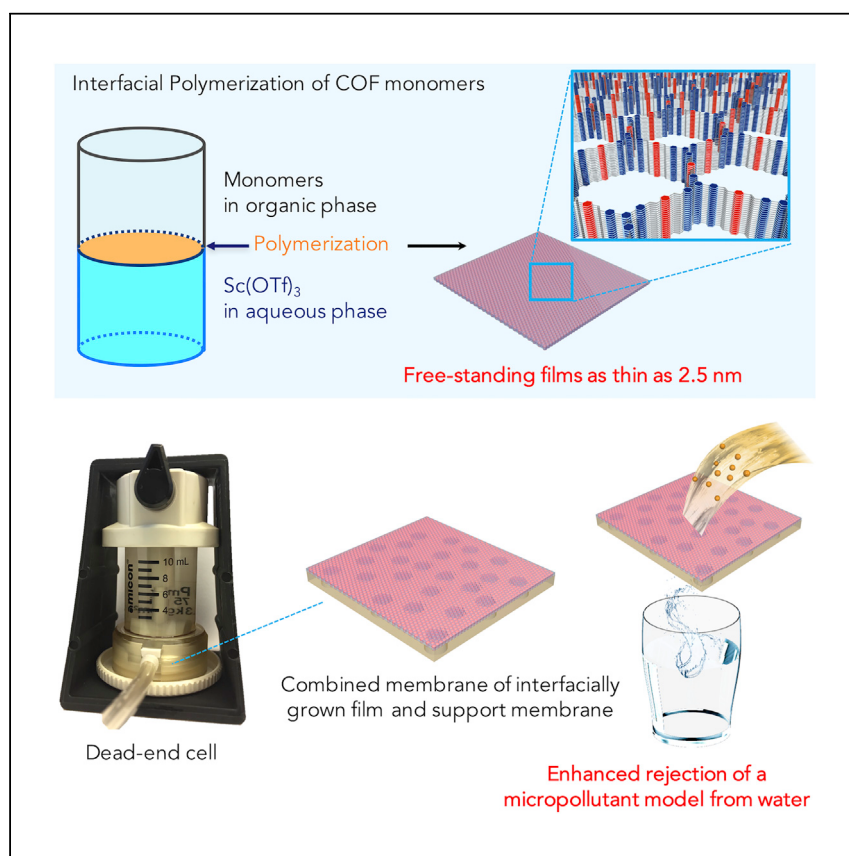


Article

Lewis-Acid-Catalyzed Interfacial Polymerization of Covalent Organic Framework Films



Interfacial polymerization with COF monomers and Sc(OTf)₃ afforded large-area (several cm²) free-standing films with tunable thickness (2.5 nm to 100 μm). When the films were thick (~100 μm), they exhibited X-ray diffraction corresponding to the expected crystalline structure. The films were integrated into the thin-film composite membranes for water nanofiltration, where they showed enhanced rejection of model pollutant Rhodamine WT.

Michio Matsumoto, Lauren Valentino, Gregory M. Stiehl, ..., Daniel C. Ralph, Benito J. Mariñas, William R. Dichtel
wdichtel@northwestern.edu

HIGHLIGHTS

The interfacial polymerization of COF monomers affords free-standing films

The film thickness is controlled by changes in monomer concentrations

The films are integrated into thin-film composite membranes for water nanofiltration



Matsumoto et al., Chem 4, 308–317
February 8, 2018 © 2017 Published by Elsevier Inc.
<https://doi.org/10.1016/j.chempr.2017.12.011>



Article

Lewis-Acid-Catalyzed Interfacial Polymerization of Covalent Organic Framework Films

Michio Matsumoto,¹ Lauren Valentino,² Gregory M. Stiehl,³ Halleh B. Balch,⁴ Amanda R. Corcos,¹ Feng Wang,⁴ Daniel C. Ralph,³ Benito J. Mariñas,² and William R. Dichtel^{1,5,*}

SUMMARY

Covalent organic frameworks (COFs) are crystalline polymers with covalent bonds in two or three dimensions, providing pores 1–5 nm in diameter. COFs are typically isolated as microcrystalline powders, which are unsuitable for many applications that would leverage their tunable structures, such as opto-electronic devices and nanofiltration membranes. Here, we report the interfacial polymerization of polyfunctional amine and aldehyde monomers with a Lewis acid catalyst, $\text{Sc}(\text{OTf})_3$. Immiscible solutions segregate the catalyst from the monomers, confining polymerization to the solution interface. This method provides large-area, continuous COF films (several cm^2) with a thickness tuned from 100 μm to 2.5 nm. Relatively thick films were crystalline, whereas the films that are a few nanometers thick were presumably amorphous. The COF films were transferred onto polyethersulfone supports, and the resulting membranes showed enhanced rejection of Rhodamine WT, a model water contaminant. The large area, tunable pore size, and tailored molecular composition show promise for nanofiltration applications.

INTRODUCTION

Two-dimensional (2D) covalent organic frameworks (COFs) are polymers that arrange polyfunctional monomers into periodic, layered structures linked by strong bonds.^{1–8} Reliable monomer design principles provide control of the COF's topology, pore size, and pore composition. These desirable features and their broad monomer scope make COFs of potential use for many applications, including gas adsorption,^{9–17} energy conversion and storage,^{18–23} proton conduction,^{24–28} and catalysis.^{21,29–32} However, most reported 2D COFs have been isolated as microcrystalline powders, which are insoluble and not easily processed into more useful forms, such that adapting them for technological applications remains challenging.

Considerable progress has been made in forming COFs as thin films,^{19,33–36} and the continued development of methods to generate free-standing COF films is an important part of these efforts.³⁷ Recently, the interfacial polymerization of monomers capable of forming imine-linked 2D COFs at air-water and liquid-liquid interfaces afforded films with thicknesses ranging from a single molecular layer to a few nanometers.^{38–40} One of the most promising features of these methods is that they provide large-area, uniform thin films, although thus far only films with amorphous or undetermined long-range order have been demonstrated. Furthermore, these methods have not used catalysts that promote imine formation or exchange. We have shown that catalysis is critical for forming imine-linked COFs,⁴¹ because the

The Bigger Picture

Two-dimensional covalent organic frameworks (COFs) are crystalline polymers with grid-like structures. COFs show promise for applications such as energy storage devices and water-purification membranes. However, their typical microcrystalline, insoluble powder form complicates or precludes their use for these applications. Here, we have formed COFs at oil-water and air-water interfaces, which provide continuous films of these materials of arbitrary size and controlled thickness. These COF films can be transferred to both solid substrates and membrane supports, and preliminary composite membranes showed rejection of model organic pollutants. This approach indicates a way forward for accessing COF films on any substrate and will enable molecular design approaches to be rationally applied to nanofiltration membranes and other applications.



monomers typically polymerize into amorphous networks that later develop long-range order through imine exchange processes. Finally, un-catalyzed liquid-liquid interfacial polymerizations require that the two monomers have orthogonal solubility, and polymerizations under Langmuir-Blodgett conditions require amphiphilic monomers and target monolayers, which impose significant design constraints.⁴⁰

Here, we report the synthesis of crystalline, free-standing COF films via the interfacial polymerization of polyfunctional amines and aldehydes in an organic solvent layered on an aqueous solution containing a Lewis acid, $\text{Sc}(\text{OTf})_3$. We recently demonstrated that $\text{Sc}(\text{OTf})_3$ is a highly active catalyst for imine-linked COF formation, which provided powder samples with outstanding crystallinity and surface area at room temperature.⁴² This catalyst is highly water tolerant and accelerates imine formation to such a degree that polymerization is limited to the interface even when both monomers are dissolved in the organic phase. This approach provides continuous films of 2D imine-linked COFs whose lateral dimensions are determined by the size of the polymerization vessel. The film thickness is controlled by the initial monomer concentration and ranges from 10 μm at monomer concentrations typically used for COF powder formation,^{41,42} to uniform, 2.5-nm-thick, polymer films when synthesized with lower monomer concentrations. The films are readily transferred to arbitrary substrates, and even the thinnest films retain their integrity when suspended over the >2 μm diameter holes of transmission electron microscopy (TEM) grids.

We also report a process to incorporate interfacially polymerized COF films into polyethersulfone (PES)-supported nanofiltration (NF) membranes and demonstrate rejection of a Rhodamine dye as a model organic pollutant. COF films are attractive for membrane filtration applications because their pores form one-dimensional channels of tunable size and chemical composition.^{43–46} This promise was recognized by Banerjee and coworkers,⁴⁷ who formed a COF solid by baking a dense mixture of monomers and an acid catalyst, which partially rejected model organic pollutants from water. However, these solids were 200–700 μm thick and cannot easily be integrated into thin-film composite (TFC) membranes (typically <250 nm) used in NF and reverse osmosis. 2D COFs polymerized at the liquid-liquid interface under $\text{Sc}(\text{OTf})_3$ -catalyzed conditions offer thickness control and transfer protocols for NF membranes that promise to leverage the outstanding structural versatility of COF molecular design approaches. These findings represent progress toward nanofiltration membranes with uniform and tunable porosity, which can be realized with further improvements in materials quality of the thinnest COF films. Even now, this study demonstrates a promising means of processing imine-linked COFs into devices and other application-relevant forms, which greatly broadens their potential utility.

RESULTS AND DISCUSSION

Interfacial COF Polymerization at the Liquid-Liquid Interface

Recently, we reported⁴² the high catalytic activity of metal triflates, particularly $\text{Sc}(\text{OTf})_3$, for the formation of an imine-linked COF (TAPB-PDA COF, 3) from 1,3,5-tris(4-aminophenyl)benzene (TAPB, 1) and terephthalaldehyde (PDA, 2) (Figure 1A). In contrast to typical conditions, which use $\text{CH}_3\text{CO}_2\text{H}$ catalysts and require elevated temperatures and long reaction times (e.g., 70°C, 72 hr), the $\text{Sc}(\text{OTf})_3$ -catalyzed polymerization occurs rapidly (10–30 min) at room temperature with low catalyst loading (<0.02 equiv). It also affords the quantitative formation of imine-linked 2D COFs as microcrystalline powders with a Brunauer-Emmett-Teller surface area (>2,000 m^2/g) among the highest reported.⁴² Previously, we reported that the addition of water to the COF condensation reaction system enhances the crystallinity of the resulting TAPB-PDA COF powders in a system catalyzed by $\text{CH}_3\text{CO}_2\text{H}$.⁴¹

¹Department of Chemistry, Northwestern University, Evanston, IL 60208, USA

²Safe Global Water Institute, Department of Civil and Environmental Engineering, University of Illinois at Urbana-Champaign, Urbana, IL 61801, USA

³Department of Physics, Cornell University, Ithaca, NY 14853, USA

⁴Department of Physics, University of California, Berkeley, Berkeley, CA 94720, USA

⁵Lead Contact

*Correspondence: wdichtel@northwestern.edu
<https://doi.org/10.1016/j.chempr.2017.12.011>

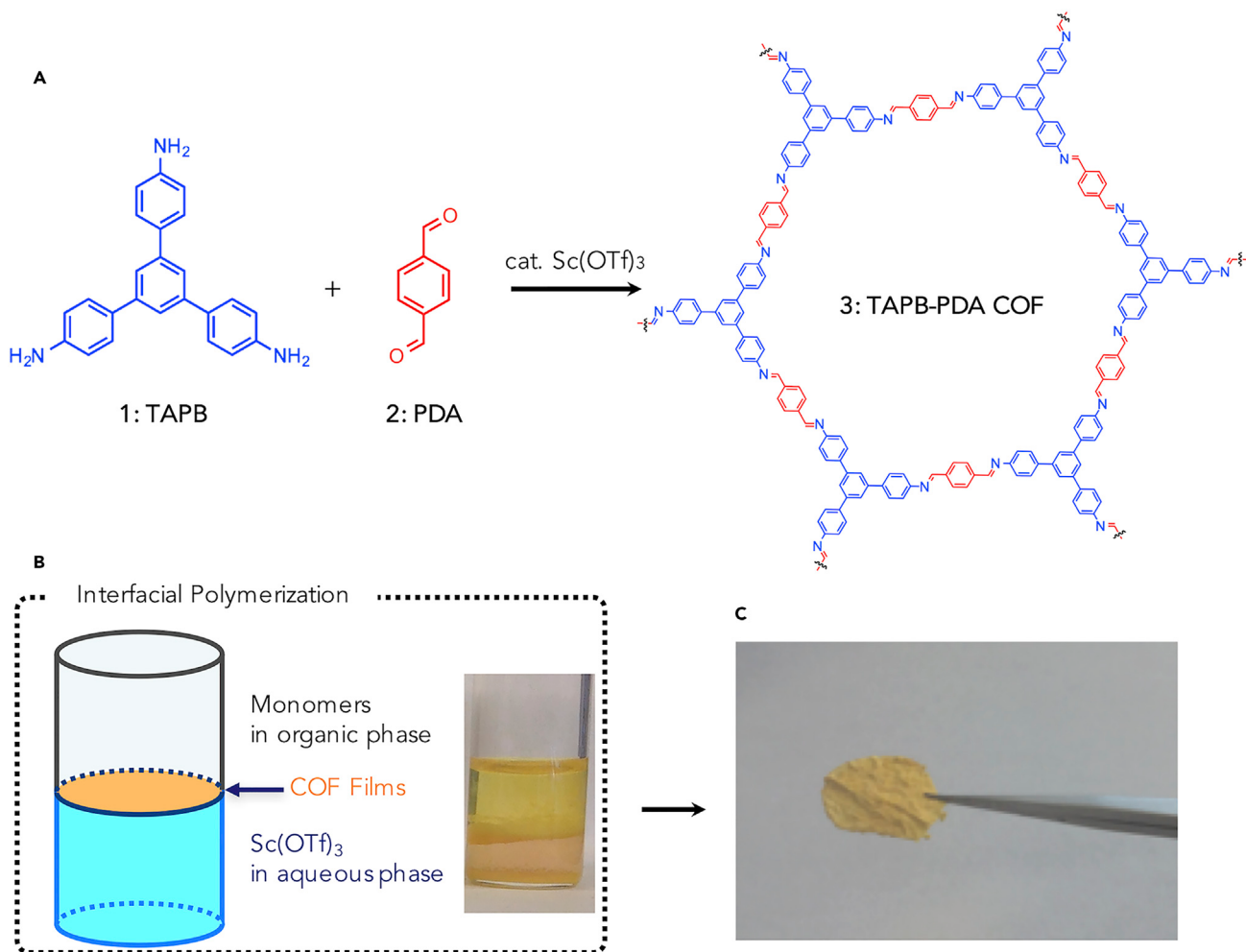


Figure 1. Interfacial Polymerization of TAPB-PDA COF

(A) Reaction scheme of TAPB-PDA COF (3) from TAPB (1,3,5-tris(4-aminophenyl)benzene) (1) and PDA (terephthalaldehyde) (2).

(B) Schematic explanation and photograph of the interfacial polymerization of TAPB-PDA COF at the interface of the organic phase and aqueous phase, which contain monomers (TAPB and PDA) and catalyst ($\text{Sc}(\text{OTf})_3$), respectively.

(C) Photo of a TAPB-PDA COF free-standing film grown by interfacial polymerization.

Following the reaction conditions suggested in our recent mechanistic study,⁴¹ we added 0.3 mL of water to a TAPB (12.5 mM) and PDA (18.8 mM) solution of 1,4-dioxane/mesitylene (4:1 v/v, 1 mL) containing a small amount of $\text{Sc}(\text{OTf})_3$ (0.001 equiv per amine). When the reaction was performed under these conditions in the absence of water, the reaction mixture became turbid within a few minutes. However, when water was added immediately after the addition of $\text{Sc}(\text{OTf})_3$, the polymerization did not proceed homogeneously but instead occurred site-selectively at the interface of the two phases to provide a polymer film. $\text{Sc}(\text{OTf})_3$ is a water-tolerant Lewis acid that is more soluble in the aqueous phase than in the organic phase. Thus, the catalyst was transferred to the aqueous phase and segregated from the COF monomers, which are preferentially soluble in the organic phase.

The spatial segregation of the catalyst and the monomers induced site-selective polymerization (see Figure 1B), which afforded a continuous film at the interface. The grown films were mechanically robust enough to be removed with tweezers without any support after a 72-hr reaction time (Figure 1C). Figure 2A shows the

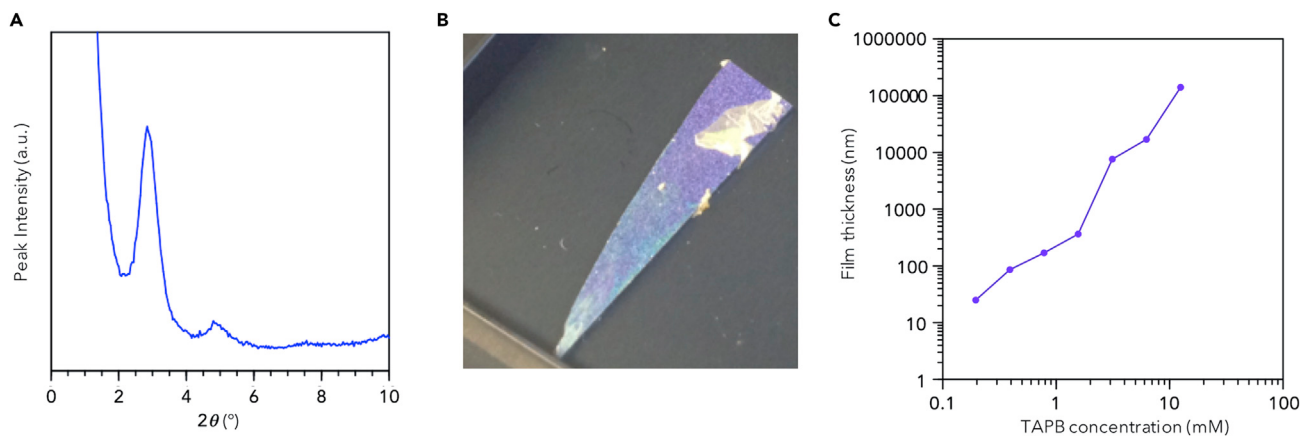


Figure 2. Effects of Monomer Concentration on Films Obtained via Interfacial Polymerization

(A) X-ray diffraction pattern of a 100-μm-thick TAPB-PDA COF film prepared with $[TAPB]_0 = 12.5$ mM and $[PDA]_0 = 18.7$ mM.

(B) Photo of a TAPB-PDA COF film (yellow) prepared with $[TAPB]_0 = 0.39$ mM and $[PDA]_0 = 0.58$ mM and transferred onto a silicon substrate.

(C) The thickness of TAPB-PDA COF films varies over several orders of magnitude according to the $[TAPB]_0$. For each film, $[PDA]_0$ was 1.5 times higher than $[TAPB]_0$ to match the 3:2 $[PDA]_0:[TAPB]_0$ molar ratio of the COF. Thicknesses are determined by either a profilometer or micrometer (for samples > 10 μm thick).

X-ray diffraction pattern of the films activated by Soxhlet extraction (CH_3OH) and subsequent supercritical CO_2 drying. The pattern we obtained was a reasonable match to that determined for the highly crystalline COF powders prepared in previous studies.⁴² Grazing-incidence wide-angle X-ray scattering (GIWAXS) measurements obtained at the Cornell High Energy Synchrotron Source (CHESS) confirmed that the COF films were highly crystalline with domains that did not exhibit an orientation.

Control of Film Thickness

The thickness of the COF film is easily tuned by variations in the initial monomer concentration. For example, we layered a 1,4-dioxane/mesitylene solution (4:1 v/v, 1 mL) of TAPB and PDA monomers at various concentrations over an aqueous solution of $\text{Sc}(\text{OTf})_3$ (300 μL, 5 mM) in a scintillation vial (2 mL). When the original monomer concentration ($[TAPB]_0 = 12.5$ mM; $[PDA]_0 = 18.8$ mM) was used, the films formed at the interface after 30 min exhibited an identical powder X-ray diffraction pattern after activation (Figure 2A).⁴² The thickness of this film was 100 μm as determined by a micrometer. In contrast, when a 64-fold lower initial monomer concentration ($[TAPB]_0 = 195$ μM; $[PDA]_0 = 293$ μM) was used as the monomer solution, the polymerization occurred more slowly but provided a thin film after 7 days. This film was transferred onto a silicon wafer by inserting the substrate underneath the interface and passing it through the grown film (Figure 2B). The film thickness was 20 nm as determined by profilometry. Figure 2C shows the relationship between the monomer concentration and the thickness of the grown films, which demonstrates that thickness can be tuned over several orders of magnitude by altering the initial monomer concentrations. This trend is similar to that observed between monomer concentration and resultant film thickness reported for the interfacial polymerization of metal organic frameworks.⁴⁸ Notably, when we layered the organic solution onto the aqueous layer too rapidly, we observed the deposition of spherical structures on top of the transferred film (Figure S4). We attribute these structures to the presence of aqueous emulsion droplets near the organic interface. Although the formation of these structures is undesirable and can be limited through experimental care, their formation and transfer to the lateral films strongly support the hypothesis that polymerization occurs selectively at the aqueous-organic interface.

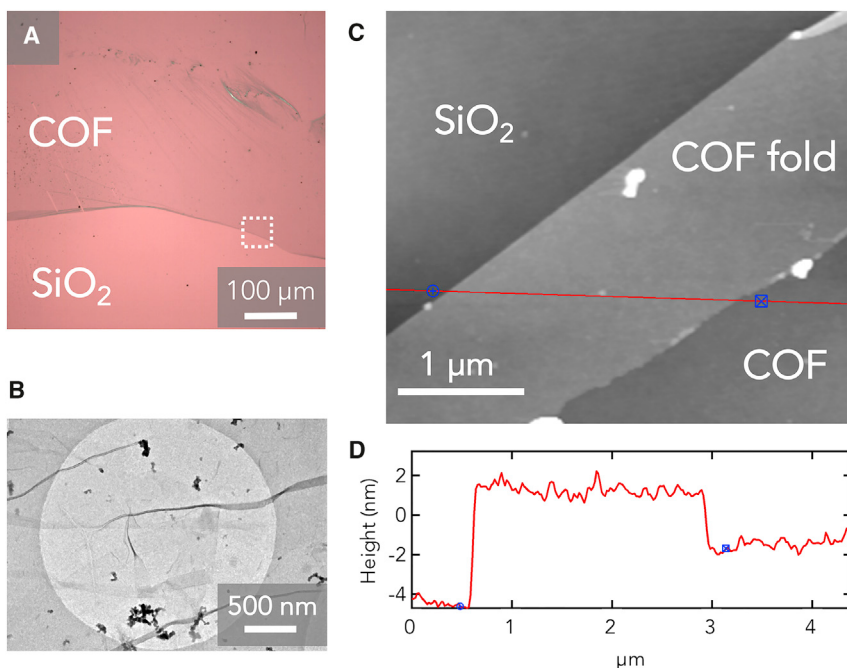


Figure 3. Microscopic Visualization and Analysis of Transferred TAPB-PDA COF Films

(A and B) Optical (A) and TEM (B) micrographs of a transferred TAPB-PDA COF film grown with a reduced amount (15.6 μL) of TAPB (1.6 mM) and PDA (2.3 mM) solution over 30 min. (C and D) AFM image (white box in A) of the transferred film (C) and a height profile (D) along the red line in (C). We transferred the TAPB-PDA COF film by scooping the film from below the aqueous-organic interface. TEM carbon grids and silicon wafer substrates were used for TEM analyses and optical-microscope and AFM analyses, respectively.

We reduced the film thickness by decreasing the concentration of monomers in the organic phase, but the reduced monomer concentration induced slower polymerizations. By adding only a small volume of the organic solution (~15 μL) to the aqueous layer, we observed rapid formation of a film a few nanometers thick within a short reaction time (30 min). After 30 min, the grown film was transferred onto a silicon wafer substrate or a carbon grid as described above. We obtained large-area, centimeter-scale COF thin films as determined through optical, atomic force microscopy (AFM), and TEM. The optical and electron micrographs in Figures 3A and 3B show that the COF films are both continuous and homogeneous on a centimeter scale. Figure 3C shows an AFM image of the edge of the film in Figure 3A where the flat sheet is visualized with folded edges (white box in Figure 3A). The cross-section (Figure 3D) along the red line in Figure 3C indicates the presence of two steps (5.5 and 2.5 nm). The image suggests that the higher feature is a folded edge of the 2.5- to 3-nm-thick film. Similar folding is observed in the TEM micrograph in Figure 3B. Given the small volume of organic solvent used in this procedure, we speculate that the reduced reaction times are attributable to the reaction taking place at a confined air-water interface that has a high local monomer concentration in the presence of the Sc(OTf)₃ catalyst compared with when larger volumes of organic solvent are used.

The 2.5-nm-thick films exhibit spectroscopic signatures consistent with the expected imine-linked COF structure. The Fourier-transform infrared spectrum of the film indicated the presence of imine linkages and was similar to that observed for the bulk crystalline COF (Figure S6). The optical absorption spectrum of the film shows a

significant red shift compared with TAPB and PDA (Figure S7), which is also characteristic of imine formation in model compounds. Although thicker films are crystalline as determined by a benchtop powder X-ray diffractometer, the films a few nanometers thick have not shown evidence of long-range order. We attempted selected area electron diffraction in TEM, low-dose high-resolution scanning TEM, and GIWAXS at the CHESS, none of which indicated evidence of crystallinity. Therefore, we conclude that the thinnest COF films are most likely amorphous. However, analysis of COFs in this form is challenging because of their large real-space lattice spacings (small reciprocal lattice spacings), susceptibility to beam damage, and small scattering cross-section of constituent atoms (carbon and nitrogen). These challenges currently limit the characterization of few-layer or single-layer 2D polymers in general.⁴⁹ The results of our previous mechanistic study suggest that the crystallinity of TAPB-PDA COFs can be enhanced by subjecting the films to reaction conditions that increase the dynamic behavior of imines.⁴¹ Such reaction conditions will be applied to the films in future studies.

Integration into Nanofiltration Membrane for Water Purification

Commercially available NF membranes are composed of three layers: a thin active layer (typically <250 nm)^{50,51} that serves as the primary barrier to water contaminants, an ultrafiltration support (~50 µm), and a thick non-woven polyester fabric for mechanical strength.⁵² The interfacial polymerization COF growth method demonstrated above is attractive because we can easily modulate the thickness of the thin active layer. We constructed the first TFC membrane consisting of a COF active layer formed via interfacial polymerization. The COF-PES membrane was formed by placing a PES support in the bottom of a reactor (Figure S8) followed by layering an aqueous $\text{Sc}(\text{OTf})_3$ solution (5 mM, 0.5 mL) and a 1,4-dioxane/mesitylene (4:1 v/v) mixed solvent solution (0.5 mL) containing TAPB (1.56 mM) and PDA (2.34 mM). After 30 min, the COF film that formed at the interface between the immiscible aqueous and organic phases was transferred onto the supporting PES membrane by drawing the reaction mixture through the bottom of the reactor. The resulting COF-PES membrane was subsequently washed carefully with methanol.

The performance of the pristine PES and the resultant COF-PES membranes was evaluated with a dead-end filtration cell (Figure 4A) for measuring the rejection of Rhodamine WT (R-WT; Figure 4B), a model compound for organic contaminants. R-WT concentrations in the permeate and the retentate were measured by fluorometry, and the rejection capabilities of the original PES and COF-PES membranes were compared over a range of membrane permeate fluxes. Note that the permeate flux, $(\text{m}^3/\text{day})/\text{m}^2$, is defined as the volumetric flow rate (m^3/day) normalized by the effective membrane area (m^2) and simplifies to m/day . Figure 4C shows that rejection depends on the permeate flux of the pristine PES and COF-PES membranes. Compared with PES alone, the COF-PES membranes showed enhanced R-WT rejection up to 91%. Furthermore, the data in Figure 4C correspond to the characterization of the same pieces of PES membrane before (PES support) and after the COF formation reaction (COF membrane). The repeat analyses demonstrated that the enhanced rejection obtained with the COF-PES membranes is reproducible despite the variability observed with the PES, which is common for commercially available membranes. This suggests the rejection of COF-PES membranes is dominated by the COF film, and the COF film rejection is highly reproducible in comparison with the commercially available PES membrane. The increase in R-WT rejection was coupled with a loss in water permeability (Figure S9) attributed in part to damage to the PES support caused by the 1,4-dioxane/mesitylene solvent mixture. Despite the decreased water permeability, this enhanced rejection is notable

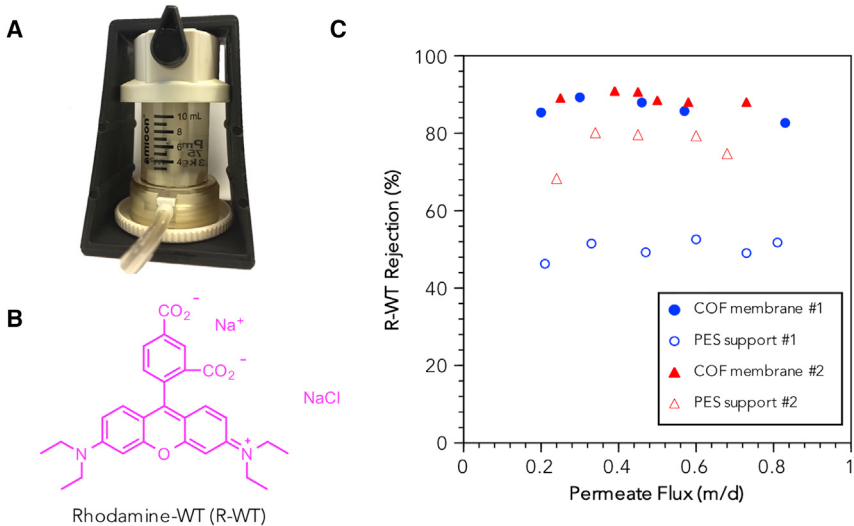


Figure 4. Rejection Tests of COF-PES Combined Membranes

(A) Photo of a dead-end stirred cell used in the rejection tests. The effective membrane area is 4.1 cm^2 .

(B) Chemical structure of Rhodamine WT (R-WT), which was used as a model compound for small organic contaminants in water.

(C) Flux-dependent R-WT rejection by polyethersulfone (PES) and COF-PES membranes. The R-WT rejection by PES membranes (open blue circle and open red triangle) was measured before and after interfacial polymerization of the COF active layer to form the thin-film composite (TFC) COF-PES membranes (solid blue circle and solid red triangle). The same protocol was used for preparing each COF-PES membrane. Experiments were performed with 2.5 mg/L R-WT as the feed solution and at varying hydraulic pressures ($0.01\text{--}0.3\text{ MPa}$) such that each pressure corresponded to a different volumetric flow rate (m^3/day), which was normalized by the effective membrane area (m^2) to give the permeate flux (m/day).

because it represents the first successful use of a selective and reproducible COF TFC membrane. Because the COF films on PES are too rough for AFM measurements, the COF films were synthesized in the same reactor and transferred to silicon wafer substrates. There, they reach a thickness of approximately 40 nm , consistent with the thickness of films synthesized with larger volumes of organic solvents for interfacial polymerization. Another point to note is that solute rejection is influenced by other factors in addition to solute size and membrane pore size, including charge interactions and solute-membrane interactions. These complexities are due to a combination of diffusive and convective components that govern solute transport across a membrane. COF-based membranes would provide opportunities to address these complexities in a rational way.⁵³ We are now investigating the rejection of additional solutes and how the COF structure and pore functionalization influence membrane performance.

Conclusions

We report free-standing film formation of TAPB-PDA COFs via interfacial polymerization catalyzed by $\text{Sc}(\text{OTf})_3$. The film thickness is modulated to several nanometers by changing the monomer concentration and/or the volume of the organic phase. The thickest film prepared ($\sim 100\text{ }\mu\text{m}$) shows an X-ray diffraction pattern that matches that of the COF powder. These examples are the first for interfacially grown films, which show X-ray diffraction patterns similar to those of powder frameworks. Interfacially polymerized COF films were incorporated as the active layer of a TFC membrane for NF treatment of aqueous solutions. The assembled membranes exhibit high rejection (up to 91%) of R-WT, a model compound for micropollutants in water.

Notably, these reaction conditions do not impose additional design constraints of the COF monomers, such as the need to dissolve the monomers in different phases. These desirable features suggest that the interfacial polymerization of imine-linked COFs with $\text{Sc}(\text{OTf})_3$ will be applicable to other COF systems, including electronically active COFs.³⁸

EXPERIMENTAL PROCEDURES

All the procedures for experiments are given in the [Supplemental Information](#).

SUPPLEMENTAL INFORMATION

Supplemental Information includes Supplemental Experimental Procedures and nine figures and can be found with this article online at <https://doi.org/10.1016/j.chempr.2017.12.011>.

ACKNOWLEDGMENTS

W.R.D., F.W., and D.C.R. acknowledge the United States Army Research Office for a Multidisciplinary University Research Initiative award under grant number W911NF-15-1-0447. W.R.D. was also supported by the Camille and Henry Dreyfus Foundation through a Camille Dreyfus Teacher-Scholar Award. We also made use of the Cornell Center for Materials Research Shared Facilities, which are supported through the National Science Foundation (NSF) Materials Research Science and Engineering Center program (DMR-1719875). This work was based upon research conducted at the Cornell High Energy Synchrotron Source, which is supported by the NSF and NIH National Institute of General Medical Sciences (DMR-1332208). This material was also based upon work supported by the NSF under grant no. CBET-1706219. We thank Hans Bechtel. This research used resources of the Advanced Light Source, which is a Department of Energy Office of Science User Facility under contract no. DE-AC02-05CH11231. Work at the Molecular Foundry was supported by the Basic Energy Sciences program of the US Department of Energy Office of Science under contract no. DE-AC02-05CH11231. The opinions in this paper do not necessarily reflect those of the sponsor.

AUTHOR CONTRIBUTIONS

Conceptualization, all authors; Methodology, M.M. and L.V.; Investigation, M.M., L.V., G.M.S., H.B.B., and A.R.C.; Writing, all authors; Funding Acquisition and Supervision, F.W., D.C.R., B.J.M., and W.R.D.

DECLARATION OF INTERESTS

The authors declare no competing interests.

Received: August 2, 2017

Revised: November 13, 2017

Accepted: December 15, 2017

Published: January 18, 2018

REFERENCES AND NOTES

1. Feng, X., Ding, X., and Jiang, D. (2012). Covalent organic frameworks. *Chem. Soc. Rev.* 41, 6010–6022.
2. Ding, S.Y., and Wang, W. (2013). Covalent organic frameworks (COFs): from design to applications. *Chem. Soc. Rev.* 42, 548–568.
3. Colson, J.W., and Dichtel, W.R. (2013). Rationally synthesized two-dimensional polymers. *Nat. Chem.* 5, 453–465.
4. Xiang, Z.H., Cao, D.P., and Dai, L.M. (2015). Well-defined two dimensional covalent organic polymers: rational design, controlled syntheses, and potential applications. *Polym. Chem.* 6, 1896–1911.
5. Waller, P.J., Gandara, F., and Yaghi, O.M. (2015). Chemistry of covalent organic frameworks. *Acc. Chem. Res.* 48, 3053–3063.

6. DeBlase, C.R., and Dichtel, W.R. (2016). Moving beyond boron: the emergence of new linkage chemistries in covalent organic frameworks. *Macromolecules* 49, 5297–5305.
7. Bisbey, R.P., and Dichtel, W.R. (2017). Covalent organic frameworks as a platform for multidimensional polymerization. *ACS Cent. Sci.* 3, 533–543.
8. Diercks, C.S., and Yaghi, O.M. (2017). The atom, the molecule, and the covalent organic framework. *Science* 355, <https://doi.org/10.1126/science.aa1585>.
9. Doonan, C.J., Tranchemontagne, D.J., Glover, T.G., Hunt, J.R., and Yaghi, O.M. (2010). Exceptional ammonia uptake by a covalent organic framework. *Nat. Chem.* 2, 235–238.
10. Rabbani, M.G., Sekizkardes, A.K., Kahveci, Z., Reich, T.E., Ding, R., and El-Kaderi, H.M. (2013). A 2D mesoporous imine-linked covalent organic framework for high pressure gas storage applications. *Chem. Eur. J.* 19, 3324–3328.
11. Huang, N., Chen, X., Krishna, R., and Jiang, D. (2015). Two-dimensional covalent organic frameworks for carbon dioxide capture through channel-wall functionalization. *Angew. Chem. Int. Ed.* 54, 2986–2990.
12. Huang, N., Krishna, R., and Jiang, D. (2015). Tailor-made pore surface engineering in covalent organic frameworks: systematic functionalization for performance screening. *J. Am. Chem. Soc.* 137, 7079–7082.
13. Li, Z., Zhi, Y., Feng, X., Ding, X., Zou, Y., Liu, X., and Mu, Y. (2015). An azine-linked covalent organic framework: synthesis, characterization and efficient gas storage. *Chem. Eur. J.* 21, 12079–12084.
14. Stegbauer, L., Hahn, M.W., Jentys, A., Savasci, G., Ochsenfeld, C., Lercher, J.A., and Lotsch, B.V. (2015). Tunable water and CO₂ sorption properties in isostructural azine-based covalent organic frameworks through polarity engineering. *Chem. Mater.* 27, 7874–7881.
15. Kang, Z.X., Peng, Y.W., Qian, Y.H., Yuan, D.Q., Addicoat, M.A., Heine, T., Hu, Z.G., Tee, L., Guo, Z.G., and Zhao, D. (2016). Mixed matrix membranes (MMMs) comprising exfoliated 2D covalent organic frameworks (COFs) for efficient CO₂ separation. *Chem. Mater.* 28, 1277–1285.
16. Ge, R., Hao, D., Shi, Q., Dong, B., Leng, W., Wang, C., and Gao, Y. (2016). Target synthesis of an Azo (N=N) based covalent organic framework with high CO₂-over-N₂ selectivity and benign gas storage capability. *J. Chem. Eng. Data* 61, 1904–1909.
17. Zhao, S., Dong, B., Ge, R., Wang, C., Song, X., Ma, W., Wang, Y., Hao, C., Guo, X., and Gao, Y. (2016). Channel-wall functionalization in covalent organic frameworks for the enhancement of CO₂ uptake and CO₂/N₂ selectivity. *RSC Adv.* 6, 38774–38781.
18. DeBlase, C.R., Silberstein, K.E., Truong, T.T., Abruna, H.D., and Dichtel, W.R. (2013). beta-Ketoenamine-linked covalent organic frameworks capable of pseudocapacitive energy storage. *J. Am. Chem. Soc.* 135, 16821–16824.
19. DeBlase, C.R., Hernandez-Burgos, K., Silberstein, K.E., Rodriguez-Calero, G.G., Bisbey, R.P., Abruna, H.D., and Dichtel, W.R. (2015). Rapid and efficient redox processes within 2D covalent organic framework thin films. *ACS Nano* 9, 3178–3183.
20. Mulzer, C.R., Shen, L., Bisbey, R.P., McKone, J.R., Zhang, N., Abruna, H.D., and Dichtel, W.R. (2016). Superior charge storage and power density of a conducting polymer-modified covalent organic framework. *ACS Cent. Sci.* 2, 667–673.
21. Xu, F., Jin, S., Zhong, H., Wu, D., Yang, X., Chen, X., Wei, H., Fu, R., and Jiang, D. (2015). Electrochemically active, crystalline, mesoporous covalent organic frameworks on carbon nanotubes for synergistic lithium-ion battery energy storage. *Sci. Rep.* 5, 8225.
22. Xu, F., Xu, H., Chen, X., Wu, D., Wu, Y., Liu, H., Gu, C., Fu, R., and Jiang, D. (2015). Radical covalent organic frameworks: a general strategy to immobilize open-accessible polyyradicals for high-performance capacitive energy storage. *Angew. Chem. Int. Ed.* 54, 6814–6818.
23. Lin, G., Ding, H., Yuan, D., Wang, B., and Wang, C. (2016). A pyrene-based, fluorescent three-dimensional covalent organic framework. *J. Am. Chem. Soc.* 138, 3302–3305.
24. Chandra, S., Kundu, T., Kandambeth, S., Babarao, R., Marathe, Y., Kunjir, S.M., and Banerjee, R. (2014). Phosphoric acid loaded azo (N=N)-based covalent organic framework for proton conduction. *J. Am. Chem. Soc.* 136, 6570–6573.
25. Xu, H., Tao, S., and Jiang, D. (2016). Proton conduction in crystalline and porous covalent organic frameworks. *Nat. Mater.* 15, 722–726.
26. Huang, C., Fu, W., Li, C.Z., Zhang, Z., Qiu, W., Shi, M., Heremans, P., Jen, A.K., and Chen, H. (2016). Dopant-free hole-transporting material with a C₃H symmetrical truxene core for highly efficient perovskite solar cells. *J. Am. Chem. Soc.* 138, 2528–2531.
27. Chandra, S., Kundu, T., Dey, K., Addicoat, M., Heine, T., and Banerjee, R. (2016). Interplaying intrinsic and extrinsic proton conductivities in covalent organic frameworks. *Chem. Mater.* 28, 1489–1494.
28. Shinde, D.B., Aiappa, H.B., Bhadra, M., Biswal, B.P., Wedge, P., Kandambeth, S., Garai, B., Kundu, T., Kurungot, S., and Banerjee, R. (2016). A mechanochemically synthesized covalent organic framework as a proton-conducting solid electrolyte. *J. Mater. Chem. A*, 4, 2682–2690.
29. Ding, S.Y., Gao, J., Wang, Q., Zhang, Y., Song, W.G., Su, C.Y., and Wang, W. (2011). Construction of covalent organic framework for catalysis: Pd/COF-LZU1 in Suzuki-Miyaura coupling reaction. *J. Am. Chem. Soc.* 133, 19816–19822.
30. Vyas, V.S., Haase, F., Stegbauer, L., Savasci, G., Podjaski, F., Ochsenfeld, C., and Lotsch, B.V. (2015). A tunable azine covalent organic framework platform for visible light-induced hydrogen generation. *Nat. Commun.* 6, 8508.
31. Lin, S., Diercks, C.S., Zhang, Y.B., Kornienko, N., Nichols, E.M., Zhao, Y., Paris, A.R., Kim, D., Yang, P., Yaghi, O.M., and Chang, C.J. (2015). Covalent organic frameworks comprising cobalt porphyrins for catalytic CO₂ reduction in water. *Science* 349, 1208–1213.
32. Lin, G., Ding, H., Chen, R., Peng, Z., Wang, B., and Wang, C. (2017). 3D porphyrin-based covalent organic frameworks. *J. Am. Chem. Soc.* 139, 8705–8709.
33. Colson, J.W., Woll, A.R., Mukherjee, A., Levendorf, M.P., Spitzer, E.L., Shields, V.B., Spencer, M.G., Park, J., and Dichtel, W.R. (2011). Oriented 2D covalent organic framework thin films on single-layer graphene. *Science* 332, 228–231.
34. Medina, D.D., Rotter, J.M., Hu, Y., Dogru, M., Werner, V., Auras, F., Markiewicz, J.T., Knochel, P., and Bein, T. (2015). Room temperature synthesis of covalent-organic framework films through vapor-assisted conversion. *J. Am. Chem. Soc.* 137, 1016–1019.
35. Bisbey, R.P., DeBlase, C.R., Smith, B.J., and Dichtel, W.R. (2016). Two-dimensional covalent organic framework thin films grown in flow. *J. Am. Chem. Soc.* 138, 11433–11436.
36. Smith, B.J., Parent, L.R., Overholts, A.C., Beauchage, P.A., Bisbey, R.P., Chavez, A.D., Hwang, N., Park, C., Evans, A.M., Gianneschi, N.C., and Dichtel, W.R. (2017). Colloidal covalent organic frameworks. *ACS Cent. Sci.* 3, 58–65.
37. Liu, X.H., Guan, C.Z., Wang, D., and Wan, L.J. (2014). Graphene-like single-layered covalent organic frameworks: synthesis strategies and application prospects. *Adv. Mater.* 26, 6912–6920.
38. Feldblyum, J.I., McCreery, C.H., Andrews, S.C., Kurokawa, T., Santos, E.J., Duong, V., Fang, L., Ayzner, A.L., and Bao, Z. (2015). Few-layer, large-area, 2D covalent organic framework semiconductor thin films. *Chem. Commun.* 51, 13894–13897.
39. Dai, W., Shao, F., Szczerbinski, J., McCaffrey, R., Zenobi, R., Jin, Y., Schluter, A.D., and Zhang, W. (2016). Synthesis of a two-dimensional covalent organic monolayer through dynamic imine chemistry at the air/water interface. *Angew. Chem. Int. Ed.* 55, 213–217.
40. Sahabudeen, H., Qi, H., Glatz, B.A., Tranca, D., Dong, R., Hou, Y., Zhang, T., Kuttner, C., Lehnert, T., Seifert, G., et al. (2016). Wafer-sized multifunctional polyimine-based two-dimensional conjugated polymers with high mechanical stiffness. *Nat. Commun.* 7, 13461.
41. Smith, B.J., Overholts, A.C., Hwang, N., and Dichtel, W.R. (2016). Insight into the crystallization of amorphous imine-linked polymer networks to 2D covalent organic frameworks. *Chem. Commun.* 52, 3690–3693.
42. Matsumoto, M., Dasari, R.R., Ji, W., Ferante, C.H., Parker, T.C., Marder, S.R., and Dichtel, W.R. (2017). Rapid, low temperature formation of imine-linked covalent organic frameworks catalyzed by metal triflates. *J. Am. Chem. Soc.* 139, 4999–5002.
43. Zang, Y., Aoki, T., Teraguchi, M., Kaneko, T., Ma, L.Q., and Jia, H.G. (2015). Two-dimensional and related polymers: concepts, synthesis, and their potential application as separation membrane materials. *Polym. Rev.* 55, 57–89.

44. Zheng, Z., Grunker, R., and Feng, X. (2016). Synthetic two-dimensional materials: a new paradigm of membranes for ultimate separation. *Adv. Mater.* 28, 6529–6545.
45. Park, H.B., Kamcev, J., Robeson, L.M., Elimelech, M., and Freeman, B.D. (2017). Maximizing the right stuff: the trade-off between membrane permeability and selectivity. *Science* 356, <https://doi.org/10.1126/science.aab0530>.
46. Koros, W.J., and Zhang, C. (2017). Materials for next-generation molecularly selective synthetic membranes. *Nat. Mater.* 16, 289–297.
47. Kandambeth, S., Biswal, B.P., Chaudhari, H.D., Rout, K.C., Kunjattu, H.S., Mitra, S., Karak, S., Das, A., Mukherjee, R., Kharul, U.K., and Banerjee, R. (2017). Selective molecular sieving in self-standing porous covalent-organic-framework membranes. *Adv. Mater.* 29, <https://doi.org/10.1002/adma.201603945>.
48. Sakamoto, R., Yagi, T., Hoshiko, K., Kusaka, S., Matsuoka, R., Maeda, H., Liu, Z., Liu, Q., Wong, W.Y., and Nishihara, H. (2017). Photofunctionality in porphyrin-hybridized Bis(dipyrinatozinc(II)) complex micro- and nanosheets. *Angew. Chem. Int. Ed.* 56, 3526–3530.
49. Hexemer, A., and Müller-Buschbaum, P. (2015). Advanced grazing-incidence techniques for modern soft-matter materials analysis. *IUCrJ* 2, 106–125.
50. Coronell, O., Gonzalez, M.I., Marinas, B.J., and Cahill, D.G. (2010). Ionization behavior, stoichiometry of association, and accessibility of functional groups in the active layers of reverse osmosis and nanofiltration membranes. *Environ. Sci. Technol.* 44, 6808–6814.
51. Lin, L., Feng, C.C., Lopez, R., and Coronell, O. (2016). Identifying facile and accurate methods to measure the thickness of the active layers of thin-film composite membranes - a comparison of seven characterization techniques. *J. Membr. Sci.* 498, 167–179.
52. Petersen, R.J. (1993). Composite reverse-osmosis and nanofiltration membranes. *J. Membr. Sci.* 83, 81–150.
53. While this manuscript was under review, another paper that also details the formation of COF films via interfacial polymerization was published. This other system uses different COF linkages and studies thicker films (e.g., several micrometers thick) for filtration experiments. Please see Dey, K., Pal, M., Rout, K.C., Kunjattu, H.S., Das, A., Mukherjee, R., Kharul, U.K., and Banerjee, R. (2017). Selective molecular separation by interfacially crystallized covalent organic framework thin films. *J. Am. Chem. Soc.* 139, 13083–13091.

Supplemental Information

**Lewis-Acid-Catalyzed
Interfacial Polymerization
of Covalent Organic Framework Films**

Michio Matsumoto, Lauren Valentino, Gregory M. Stiehl, Halleh B. Balch, Amanda R. Corcos, Feng Wang, Daniel C. Ralph, Benito J. Mariñas, and William R. Dichtel

I. Supplemental Data Items

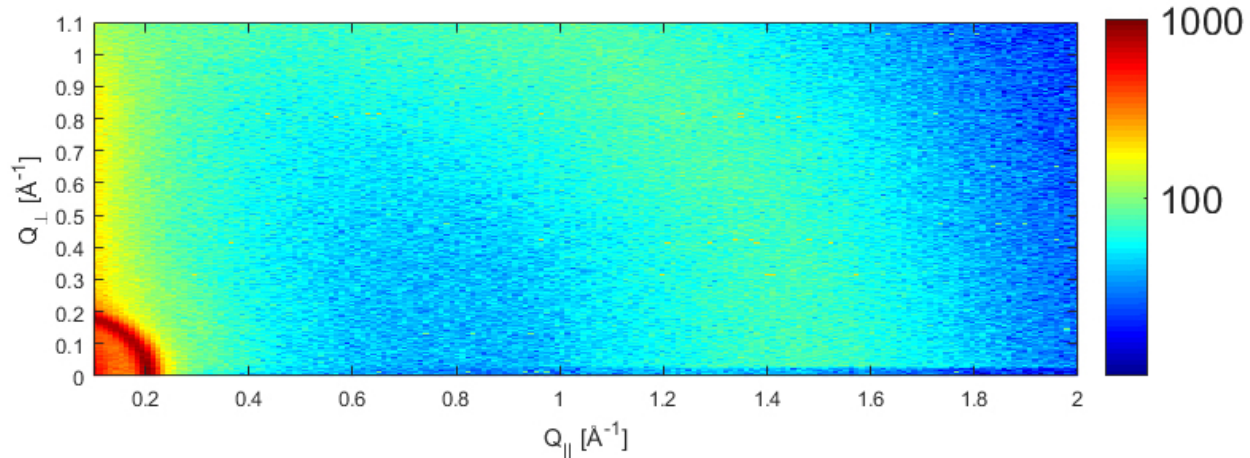


Figure S1 GIWAXS pattern of TAPB-PDA COF film grown using Condition A. The diffraction pattern indicates a crystalline network of the expected structure with randomly oriented crystalline domains.

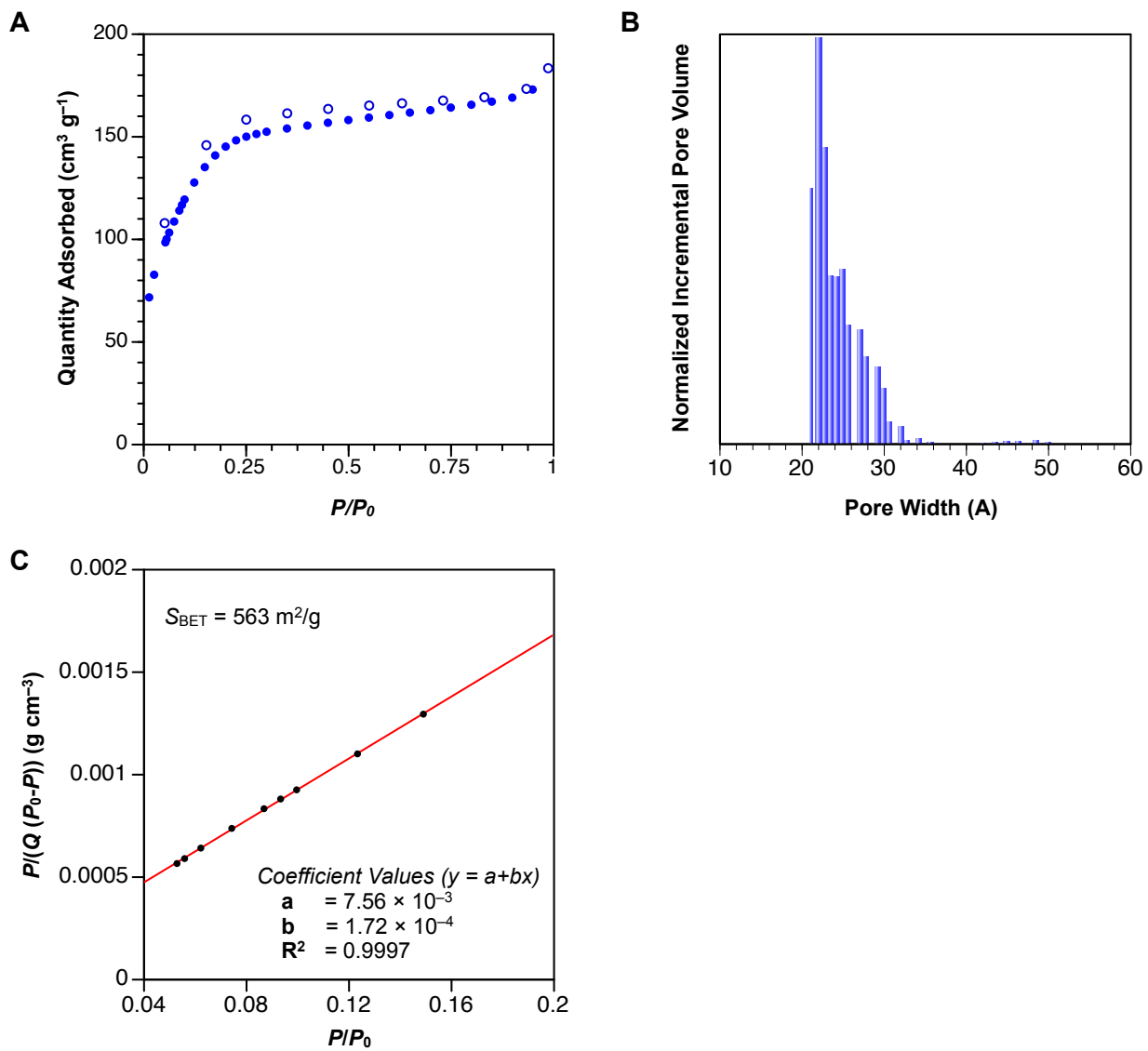


Figure S2 (A) N_2 adsorption (closed circles) and desorption (open circles) isotherms (77 K), (B) NLDFT-calculated pore size distributions, and (C) BET plot of TAPB-PDA COF film grown using Condition A.

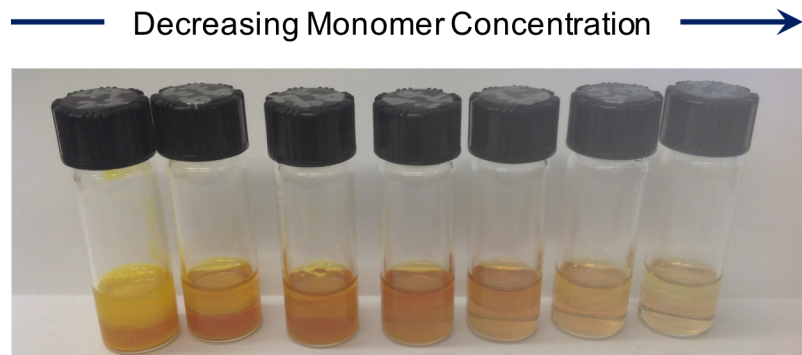


Figure S3 Photo of reaction vials for interfacial polymerization using Condition A with the modulated monomer concentrations.

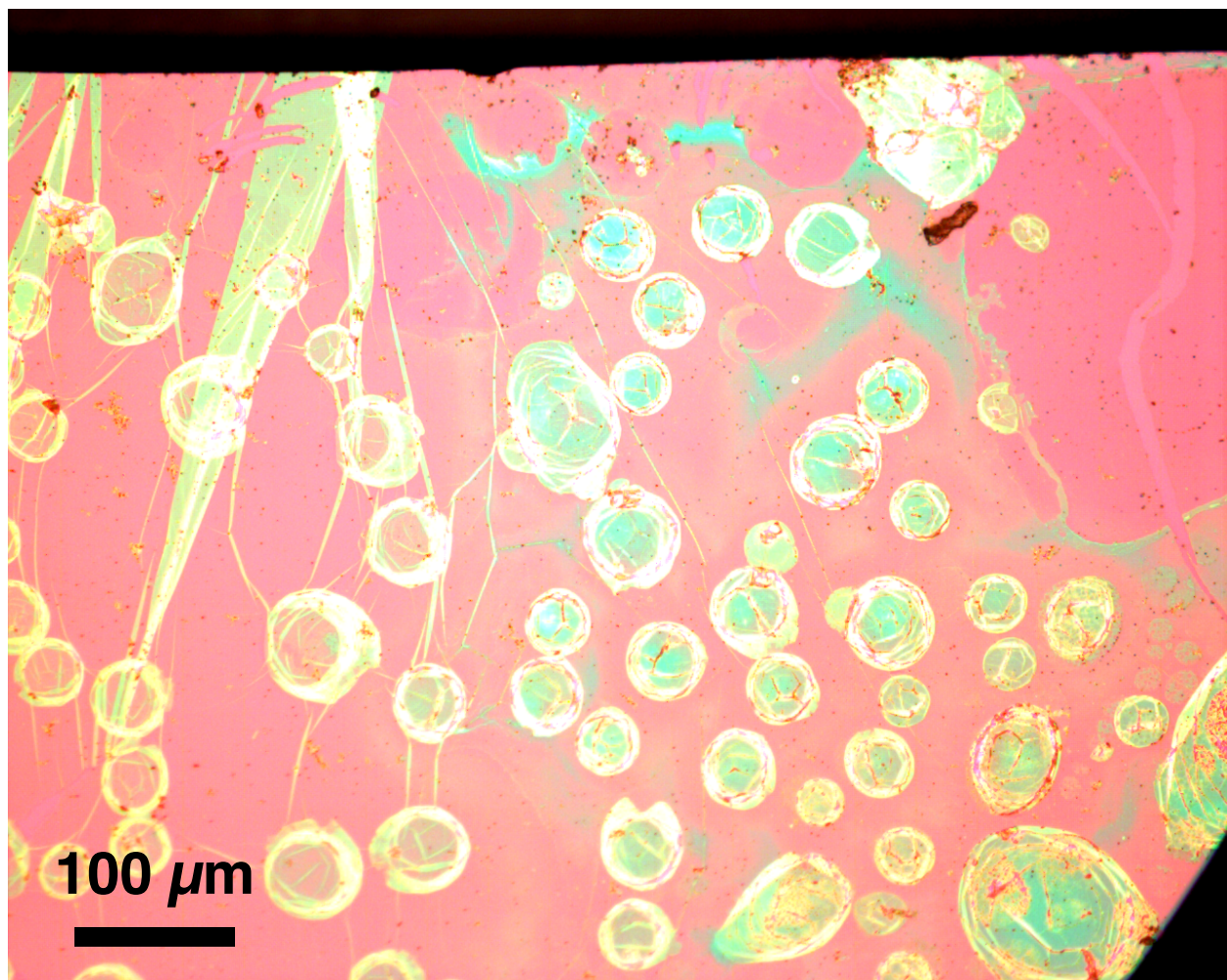


Figure S4 Optical micrograph of a film prepared under Condition A with rough layering of the two phases. We attribute the spherical structures to polymerization that occurs at the interface of droplets formed by the turbulent introduction of the organic phase.

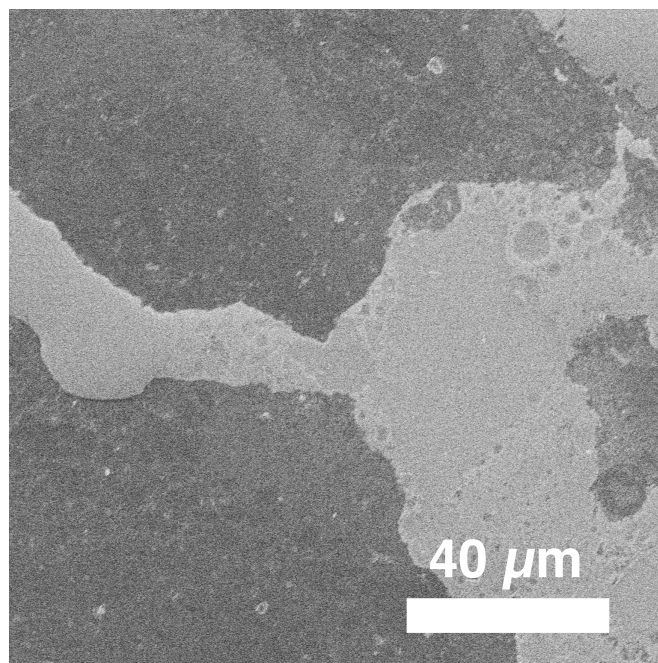


Figure S5 SEM image of TAPB-PDA COF film grown using Condition B.

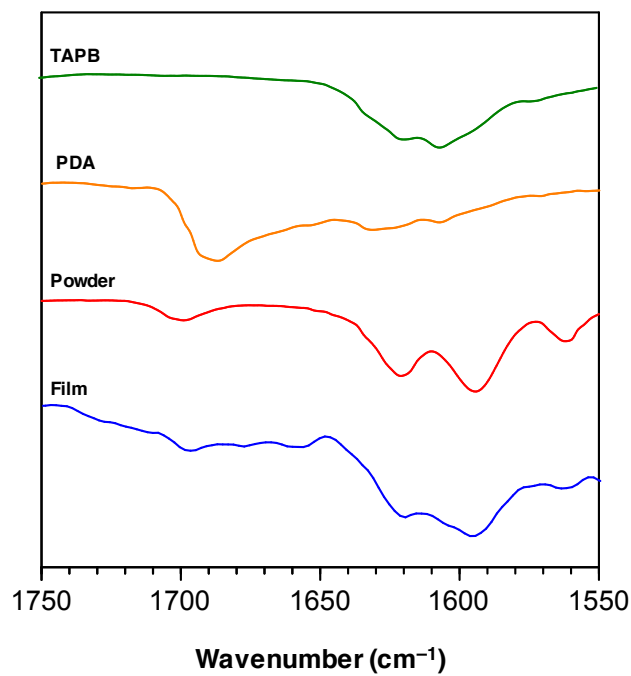


Figure S6 Partial FT-IR spectra (carbonyl/imine region) of TAPB-PDA COF films grown using Condition B (blue), TAPB-PDA COF powder grown using conditions described in ref S2 (red), PDA (orange), and TAPB (green).

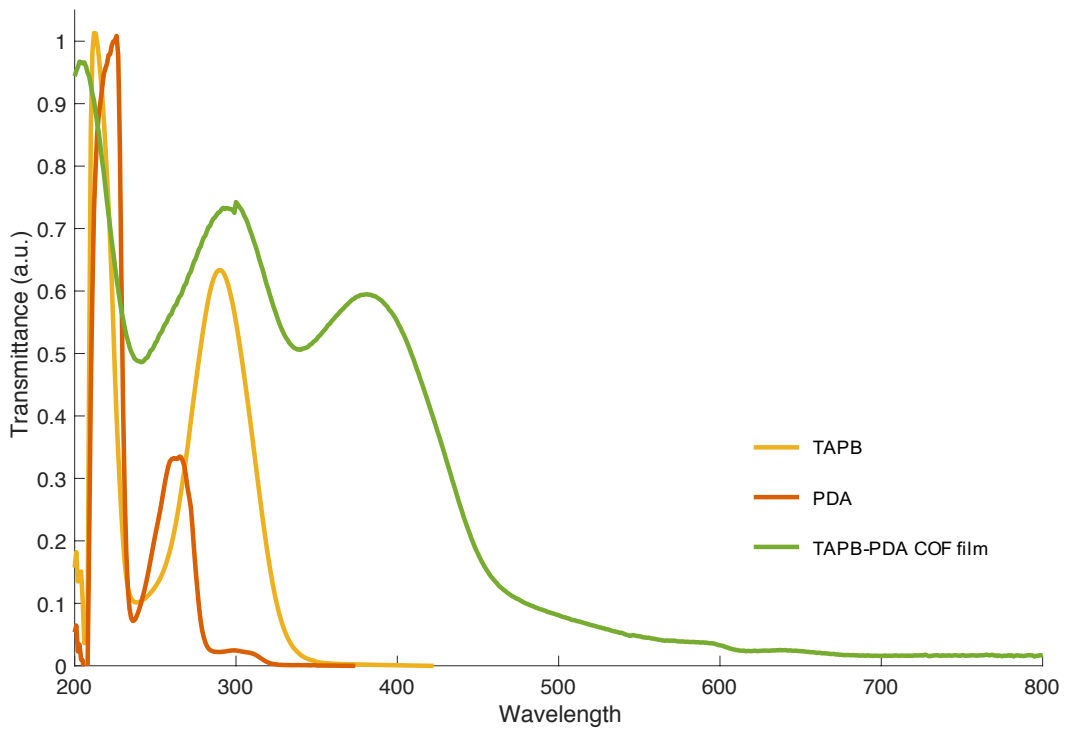


Figure S7 Optical absorption spectra of TAPB (yellow), PDA (red) and TAPB-PDA COF films grown using Condition B (green).

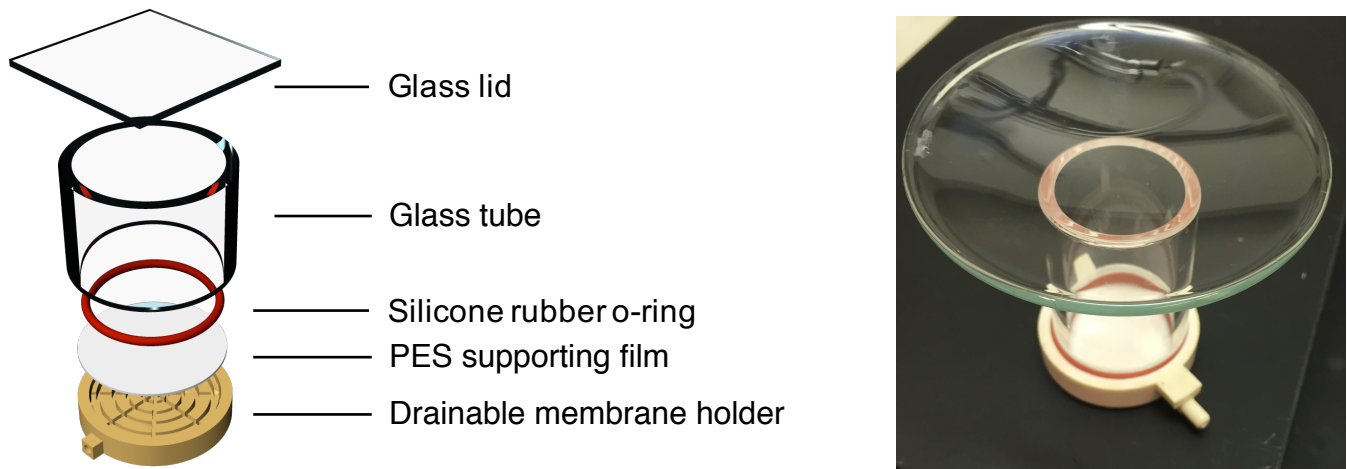


Figure S8 Schematic image and photo of reactor.

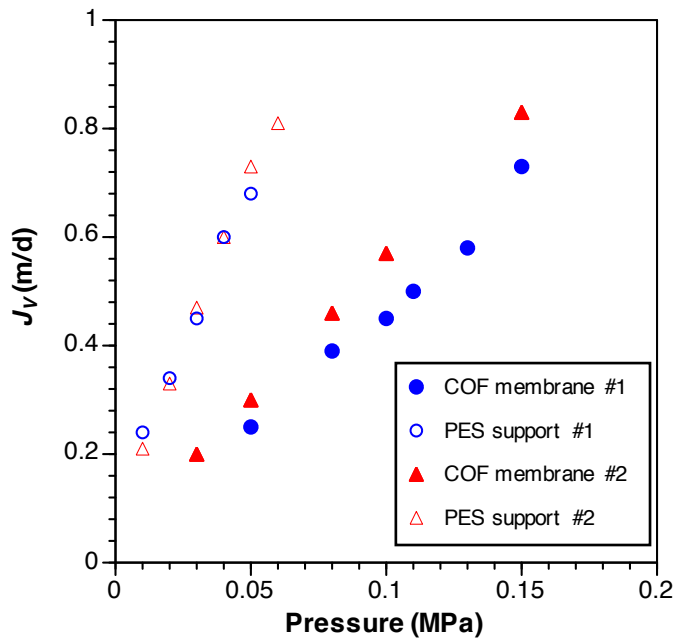


Figure S9 Water permeability for R-WT experiments (see corresponding solute rejection data in Figure 4). The water permeability by PES membranes (open blue circle and red triangle) was measured before and after interfacial polymerization of the COF active layer to form the TFC COF-PES membranes (solid blue circle and red triangle). The two COF-PES composite membranes were prepared using identical reaction conditions.

II. Supplemental Experimental Procedures

▪ Materials and Instruments

Materials:

All reagents were purchased from commercial sources and used without further purification. PES membrane model HFK-328 was purchased from Koch Membrane Systems, Wilmington, MA.

Instruments:

Supercritical CO₂ drying was conducted with a Balzers CPD 030 Critical Point Dryer.

X-ray diffraction patterns were recorded on a Scintag Powder X-Ray Diffractometer in 2θ medium resolution Brag-Brentano geometry employing Cu Kα line focused radiation at 40 kV, 44 mA power and equipped with a Ge crystal detector fitted with a 1.0 mm radiation entrance slit. Samples were mounted on zero background sample holders. No sample grinding was used prior to analysis unless otherwise noted. Samples were observed using a continuous 2θ scan from 1.0 – 12 ° (Omega = 1.0 °).

Infrared spectra were recorded on a Thermo Nicolet iS10 with a diamond ATR attachment and are uncorrected.

The optical absorption measurements were taken on a Varian 5000 UV-Vis-NIR spectrometer.

Atomic force microscopy (AFM) images were taken on an Asylum MFP-3D-BIO operating in tapping mode and equipped with a Tap150Al-G Si tip with aluminum reflex coating using a set point of 550 mV and an integral gain of 13.

Profilometry data was obtained on a Tencor Alpha Step 500 using a 5000 μm scan length and 200 Hz scan rate with 8.0 mg of stylus force.

Scanning electron microscopy (SEM) images were taken on a Hitachi S-4800 scanning electron microscope with an acceleration voltage of 5 kV.

Transmission electron microscopy (TEM) images were obtained using an FEI T12 Spirit TEM used in bright-field mode with an acceleration voltage at 80 kV.

Permeation experiments were conducted using a Millipore Amicon stirred cell model 8010.

Fluorescent spectroscopic measurements were performed on a Shimadzu RF-5301PC.

Grazing incidence X-ray diffraction (GI-XRD) was performed at the G2 station at Cornell High Energy Synchrotron Source (CHESS) using a beam energy of 10.06 ± 0.01 keV ($\lambda = 0.1232 \text{ nm}$), selected using a single-crystal Be crystal monochromator. Motorized slits were used to define a $0.2 \times 3 (\text{V} \times \text{H}) \text{ mm}^2$ beam, with a typical flux of $2 \times 10^{10} \text{ photons s}^{-1}$. The data were collected using a 640-element 1D diode-array, of which each element incorporates its own pulse counting electronics capable of count rates of $\sim 10^5 \text{ photons s}^{-1}$. A set of 0.1° Soller slits were used on the detector arm to define the in-plane resolution. The scattering geometry is described in detail elsewhere.¹ Each data set was collected by scanning the detector with the sample stationary. The incidence angle, α , between the beam and sample surface was 0.175°. Axes labels Q_{\perp} and $Q_{||}$ are defined using the GISAXS convention $Q_{\perp} = 4\pi/\lambda \sin(\delta/2)$ and $Q_{||} = 4\pi/\lambda \sin(v/2)$, where δ and v are the vertical and horizontal scattering angles, respectively. At $\alpha = \delta = 0$, $\hbar Q_{||}$ and $\hbar Q_{\perp}$ (where \hbar is

Planck's constant) are the components of momentum transfer parallel and perpendicular to the sample surface, respectively.

Surface area measurements were conducted on a Micromeritics ASAP 2020 Accelerated Surface Area and Porosimetry Analyzer using between 15 and 50 mg sample. Samples were degassed at 90 °C for 12 hours. Nitrogen isotherms were generated by incremental exposure to ultra high purity nitrogen up to ca. 1 atm in a liquid nitrogen (77 K) bath. Surface parameters were determined using BET adsorption models, and pore sizes and distributions were determined using DFT models included in the instrument software (Micromeritics ASAP 2020 V1.05).

- **Procedures for Interfacial Polymerization**

Representative procedure for the interfacial polymerization reaction (Condition A).

A stock solution of the monomers in 1,4-dioxane / mesitylene solution (4:1 v/v) was prepared according to the following procedure: 1,3,5-tris(4-aminophenyl)benzene (TAPB, 55 mg, 0.16 mmol) and terephthaldehyde (PDA, 31 mg, 0.23 mmol) were combined in a scintillation vial with a 1,4-dioxane / mesitylene solution (4:1 v/v, 6.3 mL), and the resulting suspension was sonicated at room temperature until the monomers were fully dissolved. A 1.0 mL of the stock solution was layered on top of an aqueous solution of $\text{Sc}(\text{OTf})_3$ (5 mM, 0.3 mL) in a 2 mL scintillation vial. After a 3-day reaction time, the grown film was picked up from the interface and dried under vacuum.

General procedures for screening the concentration of COF monomers.

Screening of the monomer concentration of the interfacial polymerization of COF monomers was conducted using the conditions based on Condition A. The stock solution mentioned above was diluted to various concentration with the mixed solvents (1,4-dioxane / mesitylene; 4:1 v/v) and layered as mentioned above. After a 7-day reaction time, the grown films were transferred onto silicon substrates by inserting substrates underneath of the interface and lifting the substrates up slowly.

Modified reaction conditions for shorter reaction time (Condition B)

A 15.6 μL of TAPB and PDA solution (1.56 mM and 2.34 mM, respectively) in the mixed solvent of 1,4-dioxane: mesitylene (4:1, v/v) was layered on top of an aqueous solution of $\text{Sc}(\text{OTf})_3$ (5 mM, 1.5 mL) in a 20 mL scintillation vial. After a 30-minute reaction time, the grown film was transferred onto a silicon wafer substrate or a carbon grid in the same way described above.

- **Fabrication of COF membranes and permeation experiments**

Reactor

For the interfacial polymerization of COF film and its transfer to a supporting PES membrane, the membrane holder component of a dead-end filtration cell (Amicon model 8010, EMD Millipore, Billerica, MA) was repurposed for the reactor (Figure S8). The PES substrate was placed at the bottom of the reactor, and the interfacial polymerization was designed to take place above the PES support.

Formation of COF films on top of PES support membranes

A stock solution of the monomers in 1,4-dioxane / mesitylene solution (4:1 v/v) was prepared by combining TAPB (8.8 mg, 0.025 mmol) and PDA (5.1 mg, 0.038 mmol) in a scintillation vial with a 1,4-dioxane / mesitylene solution (4:1 v/v, 1 mL), and the resulting suspension was sonicated at room temperature until the monomers were fully dissolved. A 16-fold diluted solution of the monomers was prepared using 1,4-dioxane / mesitylene solution (4:1 v/v) as the diluent. The reactor (Figure S8), containing a PES membrane (model HFK-328, Koch Membrane Systems, Wilmington, MA) at the bottom, was charged with an aqueous solution of $\text{Sc}(\text{OTf})_3$ (5 mM, 0.5 mL), and the 16-fold dilute organic solution (0.5 mL) was slowly layered on top of the aqueous layer. A glass cylinder (ID 25 mm) was placed on top of the silicone o-ring and covered with a glass plate for 30 minutes. At the end of the reaction time, the film grown by interfacial polymerization was transferred to the PES by drawing both the aqueous and organic solutions through the outlet port of the membrane holder using a needle and syringe. The COF-PES membrane was gently rinsed with MeOH and used subsequently for performance characterization.

Permeation experiments

Permeation experiments were conducted using a dead-end stirred cell (Amicon model 8010, EMD Millipore, Billerica, MA) at room temperature. Feed solutions (2.5 mg/L) of Rhodamine-WT were prepared by dilution of a concentrated solution (20% w/w, Turner Designs San Jose, CA). The feed solution pH was adjusted to 6.75 ± 0.05 using HCl or NaOH aqueous solutions prior to each experiment. Permeate flow rates were measured gravimetrically, and the data were recorded using a balance connected to a computer with a data acquisition software. Experiments were performed over a range of pressures from 0.01-0.3 MPa using nitrogen gas as the pressure source. Rhodamine-WT concentrations were determined using a spectrophotometer (RF-5301PC, Shimadzu Scientific Instruments Inc., Columbia, MD) with an excitation wavelength of 550 and emission wavelength of 580 nm.

III. References.

- S1 D. M. Smilgies, D. R. Blasini, S. Hotta, H. Yanagi, *J. Synchrotron Radiat.* **2005**, 12, 807-811.
- S2 Matsumoto, M.; Dasari, R. R.; Ji, W.; Ferriante, C. H.; Parker, T. C.; Marder, S. R.; Dichtel, W. R., *J. Am. Chem. Soc.* **2017**, 139, 4999-5002.